NeuroImage: Clinical 11 (2016) 167–172

Contents lists available at ScienceDirect

NeuroImage: Clinical

journal homepage: www.elsevier.com/locate/ynicl

Lenticulostriate arterial distribution pathology may underlie pediatric anoxic brain injury in drowning

Mariam Ishaque[a,b,*], Janessa H. Manning[c], Mary D. Woolsey[a], Crystal G. Franklin[a], Elizabeth W. Tullis[a,d], Peter T. Fox[a,b,e,f,*]

[a]Research Imaging Institute, University of Texas Health Science Center at San Antonio, 8403 Floyd Curl Drive, San Antonio, TX 78229, USA
[b]Department of Radiological Sciences, University of Texas Health Science Center at San Antonio, 7703 Floyd Curl Drive, San Antonio, TX 78229, USA
[c]Merrill Palmer Skillman Institute, Wayne State University, 71 E Ferry Street, Detroit, MI 48202, USA
[d]Conrad Smiles Fund, USA
[e]South Texas Veterans Healthcare System, 7400 Merton Minter Boulevard, San Antonio, TX 78229, USA
[f]Shenzhen University School of Medicine, Neuroimaging Laboratory, Nanhai Avenue 3688, Shenzhen, Guangong, 518060, People's Republic of China

ARTICLE INFO

Article history:
Received 25 November 2015
Received in revised form 20 January 2016
Accepted 21 January 2016
Available online 23 January 2016

Keywords:
Anoxic brain injury
Drowning
Hypoxic-ischemic brain injury
MRI
VBM

ABSTRACT

Drowning is a leading cause of neurological morbidity and mortality in young children. Anoxic brain injury (ABI) can result from nonfatal drowning and typically entails substantial neurological impairment. The neuropathology of drowning-induced pediatric ABI is not well established. Specifically, quantitative characterization of the spatial extent and tissue distribution of anoxic damage in pediatric nonfatal drowning has not previously been reported but could clarify the underlying pathophysiological processes and inform clinical management. To this end, we used voxel-based morphometric (VBM) analyses to quantify the extent and spatial distribution of consistent, between-subject alterations in gray and white matter volume. Whole-brain, high-resolution T1-weighted MRI datasets were acquired in 11 children with chronic ABI and 11 age- and gender-matched neurotypical controls (4–12 years). Group-wise VBM analyses demonstrated predominantly central subcortical pathology in the ABI group in both gray matter (bilateral basal ganglia nuclei) and white matter (bilateral external and posterior internal capsules) ($P < 0.001$); minimal damage was found outside of these deep subcortical regions. These highly spatially convergent gray and white matter findings reflect the vascular distribution of perforating lenticulostriate arteries, an end-arterial watershed zone, and suggest that vascular distribution may be a more important determinant of tissue loss than oxygen metabolic rate in pediatric ABI. Further, these results inform future directions for diagnostic and therapeutic modalities.

1. Introduction

Drowning is the third leading cause of unintentional injury death worldwide, with the highest rates among children 1–4 years old. Defined as the process of experiencing respiratory impairment from submersion/immersion in liquid, it rapidly leads to cardiac and respiratory arrest (Topjian et al., 2012). Cases of nonfatal drowning, wherein the victim successfully receives cardiopulmonary resuscitation, are also most common in children less than four years old (Borse et al., 2008; Kriel et al., 1994). For every pediatric drowning death, at least two survivors are hospitalized from a drowning incident (Weiss, 2010). In these patients, nonfatal drowning damages many organs, but the most devastating disability results from brain injury (Ibsen and Koch, 2002).

Anoxic brain injury (ABI; also hypoxic-anoxic injury) can result from nonfatal drowning and cardiac arrest as the brain is exceptionally sensitive to the duration and intensity of oxygen deprivation (Topjian et al., 2012). Often used synonymously with hypoxic-ischemic brain injury (HI-BI, a more descriptive term), ABI involves a complex constellation of injuries to the brain from hypoxia, ischemia, cytotoxicity, and combinations thereof (Busl and Greer, 2010). With these insults, the brain is deprived not only of oxygen, but also of glucose and other nutrients that support neural metabolism. This triggers injurious biochemical cascades, including excessive neurotransmitter release leading to excitotoxicity, oxygen free radical formation, lactic acidosis, and

Abbreviations: ABI, anoxic brain injury; ACA, anterior cerebral artery; CT, computerized tomography; DTI, diffusion tensor imaging; HI-BI, hypoxic-ischemic brain injury; MCA, middle cerebral artery; MNI, Montreal Neurological Institute; MPRAGE, magnetization prepared rapid gradient echo; PLIC, posterior limb of the internal capsule; VBM, voxel-based morphometry.

* Corresponding authors at: Research Imaging Institute, 8403 Floyd Curl Drive, San Antonio, TX 78229, USA. Tel.: +1 210 567 8150.
E-mail addresses: Ishaque@livemail.uthscsa.edu (M. Ishaque), janessa.manning@wayne.edu (J.H. Manning), woolseym@uthscsa.edu (M.D. Woolsey), franklinc@uthscsa.edu (C.G. Franklin), liztullis@me.com (E.W. Tullis), Fox@uthscsa.edu (P.T. Fox).

http://dx.doi.org/10.1016/j.nicl.2016.01.019

ultimately, neuronal death. Further, lactic acid and other cytotoxic agents that are normally removed by the circulation accumulate due to ischemia (Huang and Castillo, 2008). It has been widely reported that certain brain regions are more susceptible to HI-BI than others, a concept known as selective vulnerability (Huang and Castillo, 2008). Observed patterns of injury may reflect cellular metabolic demands, vascular distribution (e.g., watershed zones), or both (Hegde et al., 2011).

Several studies have concluded that brain tissues with higher densities of excitatory neurotransmitter receptors and higher metabolic demands are especially susceptible to damage from anoxic-ischemic insults (Huang and Castillo, 2008; Rabinstein and Resnick, 2009). Regions with high concentrations of glutamate or other excitatory amino acid receptors (gray matter) are more vulnerable to excitotoxicity. Increased synaptic activity in these tissues also results in greater energy demands, rapidly subjecting them to energy depletion and early injury with oxygen deprivation. Accordingly, the selective vulnerability of gray matter has been largely established across anoxic etiologies. Traditionally implicated regions include the basal ganglia, cerebellum, and hippocampi (Huang and Castillo, 2008; Rabinsten and Resnick, 2009; Souminen and Vähätalo, 2012). Movement, coordination, and memory deficits are consequently the most common sequelae in survivors (Topjian et al., 2012).

Vascular pathogenesis has also been suggested in ABI and implicates cerebral watershed regions. These border zones involve the junction of the distal fields of two nonanastomosing arterial systems and have decreased tolerance to ischemia. Classically, two distinct watershed zones are recognized: (1) cortical watershed: between the territories of the anterior, middle, and posterior cerebral arteries; and (2) internal watershed: in the white matter between the deep and superficial arterial systems of the MCA, or between the superficial systems of the MCA and ACA (Momjian-Mayor and Baron, 2005). The central subcortical gray and white matter comprising the vascular territory of the perforating lenticulostriate arteries has not collectively been proposed as a predominant site of injury with anoxia. Importantly, despite the suggested involvement of the above hypoxia-vulnerable areas, the full extent of consistent short- and long-term neuropathological consequences of drowning have yet to be established.

Neuroimaging modalities are particularly critical in the examination of post-drowning ABI, as there exist no systematic pathological (post-mortem) human studies in this disorder. CT and MRI have been extensively applied clinically following resuscitation from drowning. Acute anatomical imaging findings are often subtle or reported as normal, even in cases of severe ABI. Diffuse edema, which manifests as the loss of normal contrast between gray and white matter, is the most common early finding on CT and T1/T2-weighted MRI (Rafaat et al., 2008; Rabinsten and Resnick, 2009). Chronically, diffuse structural atrophy is frequently observed. Diffusion MRI methods are more sensitive in the detection of ABI; when focal pathology is present, basal ganglia and cerebellar damage are most commonly reported (and associated with poor outcomes) (Rabinsten and Resnick, 2009). Outcomes in pediatric nonfatal drowning can range from considerable recovery, to varying levels of neurological impairment, to minimally conscious and persistent vegetative states, to brain death (Christensen et al., 1997). Severe motor impairments, including loss of self-mobility, self-feeding, and communication capabilities are common post-drowning ABI consequences, and various movement disorders have been reported across other hypoxic-ischemic etiologies (Lu-Emerson and Khot, 2010).

It is important to note that reports of structural neuroimaging findings in pediatric ABI have relied solely on visual inspection. There exist no quantitative or group analyses of consistent gray and white matter damage with drowning. Determination of the extent, course, and uniformity of anatomical brain pathology from anoxia in these patients is necessary and could be highly valuable in establishing patterns of damaged versus intact neural tissue, in suggesting the underlying pathophysiological processes of ABI in drowning, in clinical decision making, and in informing future targeted analyses. The purpose of this paper is to use morphometry to further understand neuropathology in pediatric nonfatal drowning and make causal inferences regarding the pathophysiology of this disorder. This necessitates the use of robust structural neuro image analysis methods.

Voxel-based morphometry (VBM) is a quantitative, group-wise structural image analysis technique capable of detecting even subtle, consistent pathology across subjects (Ashburner and Friston, 2000). VBM methods have been applied to numerous neurological disorders and have successfully identified structural changes otherwise difficult to visually perceive. To date, they have not been implemented in pediatric nonfatal drowning. In the present study, we have acquired high-resolution T1-weighted MRI data in 11 children with chronic ABI and 11 age- and gender-matched neurotypical control children. We have utilized recently optimized, whole-brain VBM methods to define and quantify consistent structural pathology from nonfatal drowning among pediatric patients.

2. Materials and methods

2.1. Subjects

22 subjects were studied: 11 children with chronic ABI from nonfatal drowning, and 11 age- and gender-matched neurotypical controls. All ABI patients were medically stable, greater than six months post injury, with no contraindications to MRI, and with normal sleep–wake cycles (children were studied during sleep). The ABI cohort's range in age at injury (1.4–4.8 years) reflects the highest-risk population for accidental drowning. All ABI subjects displayed consistent, substantial motor impairments, as assessed through their ability for autonomous and purposeful movement, mobility, and speech production. Cognitive abilities appeared to vary, but were difficult to assess due to the motor impairments. All participants' parent(s) consented to the study's protocol approved by the University of Texas Health Science Center at San Antonio's Institutional Review Board.

2.2. Image Acquisition

MRI data were obtained on a 3T Siemens TIM-Trio (Siemens Medical Solutions, Erlangen, Germany), using a standard 12-channel head coil as a radiofrequency receiver and the integrated circularly polarized body coil as the radiofrequency transmitter. T1-weighted images were acquired during mildly sedated sleep (1–2 mg/kg Diphenhydramine HCl) using the MPRAGE pulse sequence with TR/TE = 2200/2.72 ms, flip angle = 13°, TI = 766 ms, volumes = 208, and 0.8 mm isotropic voxel size.

2.3. Visual inspection

Acquired images were visually inspected per subject for artifacts, non-related pathology, and/or evidence of motion. Three ABI and two control data sets showed excessive motion. Two of the ABI subjects were successfully rescanned, ultimately yielding high-quality data sets in 10 ABI and 9 control participants. ABI pathology ranged from mild ventricular enlargement, to moderate ventricular enlargement with mild basal ganglia atrophy and mild cortical thinning, to severe ventricular enlargement with severe basal ganglia atrophy and diffuse cortical thinning. See Table 1 for subject data.

2.4. Voxel-based morphometry

2.4.1. Gray matter VBM

T1 structural images were denoised using Matlab's MRI Denoising package (Optimized Nonlocal Means filter with Rician option activated) (Coupé et al., 2008, 2010). FreeSurfer was used to obtain brain-extracted images and masks following processing with *autorecon1*

Table 1
Subject data.

Group	Sex (M/F)	Age at injury (yrs)[a] (mean ± SD)	Age at scan (yrs)[a] (mean ± SD)	Time since injury (yrs)[a] (mean ± SD)	Visual inspection of MRI pathology[b] (n)
ABI n = 10	7/3	2.6 ± 1.1	7.9 ± 3.1	5.3 ± 3.3	Mild ventricular enlargement (5) Moderate ventricular enlargement, mild basal ganglia atrophy, mild cortical thinning (3) Severe ventricular enlargement, severe basal ganglia atrophy, diffuse cortical thinning (2)
Control n = 9	7/2		7.7 ± 2.1		None (9)

[a] Years.
[b] T1-weighted MRI assessed by visual inspection and categorized by extent of structural damage.

(motion correction conform, non-uniform intensity normalization, Talairach transform computation, intensity normalization, and skull stripping) (Segonne et al., 2004). Brain-extracted data was analyzed with FSL-VBM (Douaud et al., 2007), an optimized VBM protocol carried out with FSL tools (Good et al., 2001; Smith et al., 2004). Structural images were gray matter-segmented and non-linearly registered to MNI-152 standard space (Andersson et al., 2007). The resulting images were averaged, flipped along the x-axis, and re-averaged to create a left–right symmetric, study-specific gray matter template. All native gray matter images were non-linearly registered to this study-specific template and "modulated" to correct for local expansion (or contraction) due to the non-linear component of the spatial transformation. The modulated gray matter images were smoothed with an isotropic Gaussian kernel (sigma = 3 mm). To compare ABI versus control group differences in gray matter volume, voxel-wise general linear modeling was applied using permutation-based non-parametric

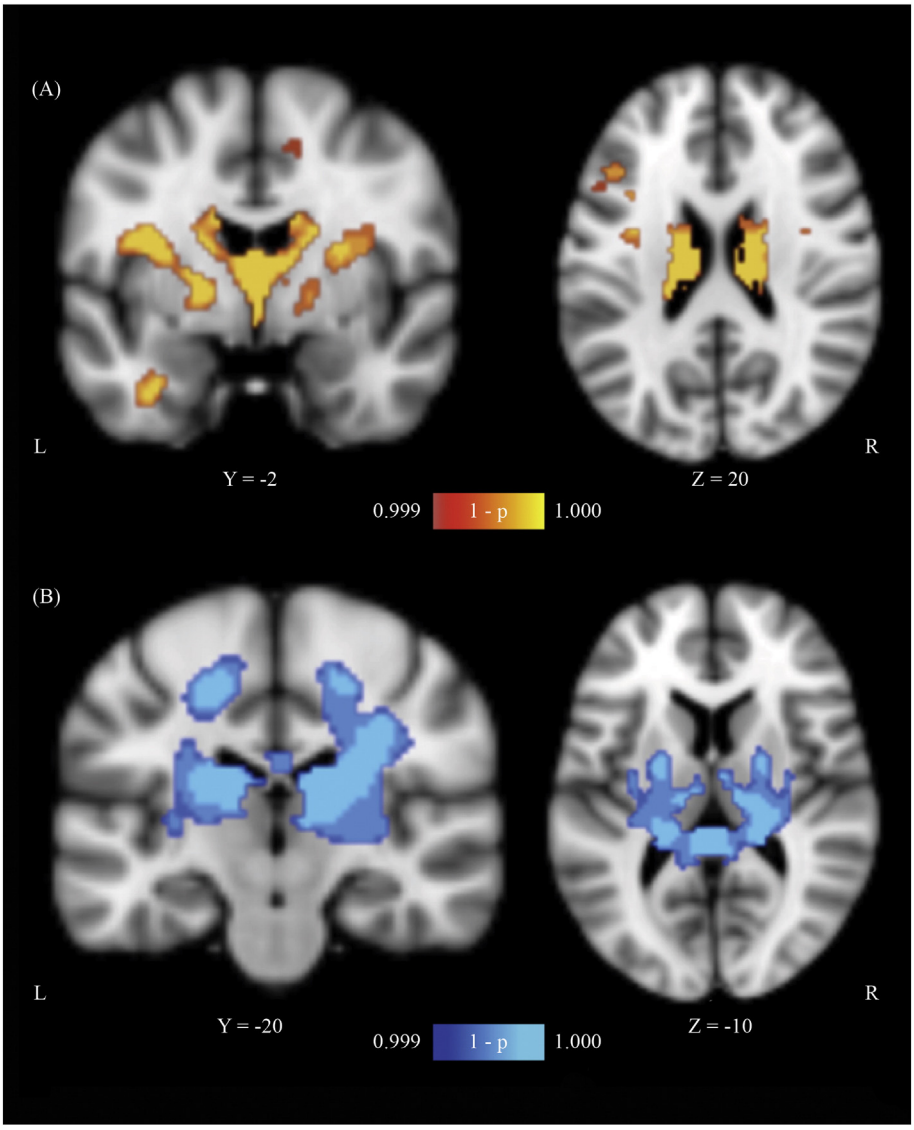

Fig. 1. Gray and White Matter VBM results. (A) Gray matter and (B) White matter VBM results (controls > patients) demonstrating areas of atrophy in the anoxic brain injury (ABI) group relative to the neurotypical control group ($P < 0.001$; corrected for multiple comparisons). Slice position (given by *y* or *z* location) corresponds to the Montreal Neurological Institute's (MN1-152) template space. *Note*: The right-hand side image in (A) is sliced at the level of the caudate body.

testing, correcting for multiple comparisons across space ($P < 0.001$). The output comprised threshold-free cluster enhancement (TFCE) based statistical parametric maps depicting locations of gray matter differences between patient and control groups. TFCE avoids the arbitrary definition of an initial cluster-forming threshold, as in cluster-based thresholding, by enhancing cluster-like structures while maintaining a voxel-wise approach (Smith and Nichols, 2009). The results were overlaid onto the MNI-152 standard template (Fig. 1A). Maxima locations were derived from the Talairach Daemon (Lancaster et al., 1997, 2000).

2.4.2. White matter VBM

White matter VBM was implemented on the preprocessed images as described above (following Matlab denoising and FreeSurfer brain extraction). FSL-VBM scripts were manually altered to specify white matter analysis in all subsequent steps. Image processing proceeded as described above for gray matter. The output comprised TFCE-based statistical parametric maps depicting locations of white matter differences between patient and control groups (Fig. 1B). Maxima locations were derived from the JHU ICBM-DTI-81 atlas (Mori et al., 2005).

3. Results

As hypothesized, our quantitative VBM methods revealed a spatially consistent pathological distribution. This was observed despite the fact that 5/10 patients with anoxic damage did not have visually apparent tissue loss on MR images.

Significant clusters of reduced gray matter volume in ABI patients relative to neurotypical controls were predominantly in the subcortical gray matter, focused around the basal ganglia nuclei (bilaterally) and the thalamus (Fig. 1A; Table 2). Additional significant areas included the cerebellum and bilateral postcentral gyri.

A significant cluster of reduced white matter volume in ABI patients relative to neurotypical controls was found surrounding subcortical nuclei and encompassing bilateral external capsules, bilateral posterior limbs of the internal capsule (PLIC), bilateral superior corona radiata, and the splenium of the corpus callosum (Fig. 1B; Table 2).

The distribution of damage overall was highly convergent on central subcortical structures, both gray and white matter. This is consistent with the vascular territory of the lenticulostriate arteries (Fig. 2). Primary involvement of the traditional watershed zones was not observed.

Table 2
VBM Results. Location and coordinates of peaks of significant gray and white matter volume decreases ($P < 0.001$, cluster size > 200 voxels).

Anatomical location	Cluster size (voxels)	Hemisphere	MNI coordinates of global maxima		
			x	Y	z
Gray matter					
Control > ABI					
Sub-lobar gray matter	8106	L	−14	−4	28
Cerebellum	570	R	10	−72	−20
Postcentral gyrus	442	R	44	−18	34
Postcentral gyrus	229	L	−42	−20	42
ABI > Control					
None					
White matter					
Control > ABI					
Superior corona radiata	8346	L	−20	−14	54
ABI > Control					
None					

Note: The sub-lobar gray matter cluster encompasses bilateral caudate, putamen, and lateral globus pallidus nuclei, and the thalamus. The gray matter clusters with maxima in the right and left postcentral gyri also comprise the right and left precentral gyri, respectively. The white matter cluster (with maximum peak in the left superior corona radiata) encompasses the right superior corona radiata, bilateral external capsules, bilateral posterior limbs of the internal capsule, and the splenium of the corpus callosum. Gray and white matter tissue labels derived from Talairach Daemon and JHU ICBM-DTI-81 atlas, respectively.

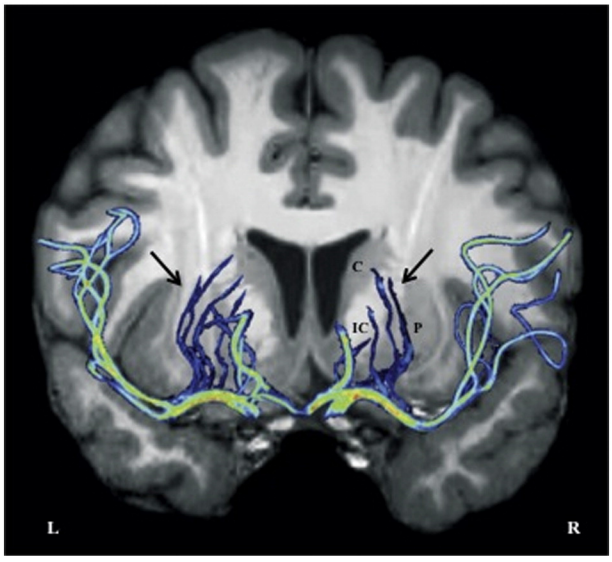

Fig. 2. Lenticulostriate arterial system. Maximum intensity projection (2D, pseudo colored) view of MR angiography image in a healthy volunteer (M.I.); overlaid on T1-weighted MR anatomical image. Arrows depict left and right lenticulostriate arterial branches supplying central subcortical gray and white matter structures. C = Caudate; *P* = Putamen; IC = Internal Capsule. *Note*: We were not able to visualize and isolate all lenticulostriate branches; their supply to the right putamen (*P*) is likely not fully depicted here.

There were no significant regions of gray or white matter atrophy in the control group relative to the ABI patient group.

4. Discussion

Predominant focal damage in the central subcortical gray and white matter was found in pediatric ABI patients, the population at highest risk for nonfatal drowning. Gray matter loss was localized to the basal ganglia nuclei (bilaterally), thalamus, cerebellum, and bilateral postcentral gyri (sensorimotor cortex). White matter loss was localized to bilateral external capsules, PLICs, and superior corona radiata, and the splenium of the corpus callosum.

4.1. Inferred ABI pathophysiology

Our findings challenge the notion that oxygen metabolic rate and excitatory neurotransmitter concentration are the primary determinants of selective vulnerability to HI-BI in pediatric nonfatal drowning. The basal ganglia nuclei (e.g., caudate, putamen, globus pallidus) are rich in mitochondria and neurotransmitters and are highly metabolically active. These properties make them particularly susceptible to global hypoxic insults, and they are often seen as affected on MR images (Hegde et al., 2011). The thalamus, cerebellum, and (to lesser extents) the sensorimotor cortex are also regularly reported as damaged with oxygen deprivation due to cellular metabolic activity levels (Huang and Castillo, 2008; Rabinstein and Resnick, 2009). However, white matter is thought to be relatively spared from pathology (Hegde et al., 2011) (or to manifest damage in a delayed manner, possibly in internal watershed regions) (Rabinstein and Resnick, 2009).

Observing comparable volume loss in subcortical gray and white matter, our results argue that the metabolic profiles of the respective neural tissues are less likely to predominantly drive pathology in drowning-related pediatric ABI. The VBM findings instead suggest pathophysiology may be driven by vascular causes, but not in a classic watershed distribution (despite some overlap in internal watershed subcortical structures; cf. Rabinstein and Resnick, 2009, Figs. 1–13). Tissue-loss topography, instead, implicates the vascular territory of the perforating lenticulostriate arteries (Fig. 2) as a result of cardiovascular

dysfunction and systemic hypotension with drowning. With lateral and medial perforating branches arising from the MCA and ACA respectively, these vessels are the dominant vascular supply of the central deep gray and white matter (Saenz, 2005). Djulejic et al. (2012, 2015) defined their territorial distribution to include (fully or partially) the caudate, putamen, globus pallidus, basal forebrain, internal and external capsules, and the corona radiata. The lenticulostriate arteries are susceptible to hypertension-related hemorrhage and embolic occlusion, and as they are end arteries, the regions they supply do not have significant collateral blood flow (Wardlaw, 2005). Based on our morphometry results, pediatric brain injury in nonfatal drowning appears to selectively target the deep gray and white matter in a manner that 1) partly reflects metabolic activity and cellular composition, but 2) largely reflects lenticulostriate arterial distribution.

Additionally, we must consider the possibility of central subcortical gray matter tissue loss as the primary consequence of the anoxic insult, and the surrounding white matter tissue loss as a secondary degenerative effect. Although such a pattern of injury is not prominently found in the literature, this is a reasonable consideration as several white matter tracts originate in the basal ganglia nuclei and thalami.

4.2. Motor-system damage

The basal ganglia nuclei comprise the extrapyramidal system and play an integral role in the production and control of voluntary movement. With reciprocal projections with the cerebral cortex and thalamus, these nuclei receive, modify, and relay motor information; lesions can thus result in substantial motor-system impairments (Anderson et al., 2004; Hegde et al., 2011). In the deep white matter adjacent to the basal ganglia, the PLIC contains corticospinal fibers that relay motor information from the primary motor cortex to lower motor neurons. The preferential involvement of cerebral motor networks is a clear implication of our VBM results. This distribution is entirely consistent with the extensive motor deficits routinely reported in this population and observed in the patient cohort reported here. Importantly, evidence of substantial damage to other neural systems – perceptual, emotive, and cognitive – is notably lacking (although disconnection in white matter tracts may extend the functional deficit.) This suggests that severe but selective motor deficits could potentially mask a level of behavioral integrity not previously suspected in this population. We hypothesize that persons with ABI secondary to pediatric nonfatal drowning are unable to effectively communicate their inner state and may be substantially less globally impaired than can be readily detected clinically. This disconcerting hypothesis demands further investigation and can be tested using the current generation of functional neuroimaging methods.

4.3. Clinical impact

In addition to the critical implications of an unexpected residual functional capacity in pediatric drowning patients (pending further investigation), our findings can inform—and potentially significantly improve—clinical management in these cases. MR spectroscopy (MRS), which provides a metabolic profile of the brain, has been useful in predicting outcomes with drowning and could supplement structural MRI observations. Previous studies suggest that 1H MRS has improved sensitivity when implemented 3–4 days post-drowning (versus 1–2 days), and that the N-Acetyl-Aspartate/Creatine (NAA/Cr) ratio and/or lactate could be potent markers for assessment and prognosis in acute drowning (Aragao et al., 2009; Gutierrez et al., 2010; Nucci-Da-Silva and Amaro, 2009; Topjian et al., 2012). For optimal impact and reasonable scan times, however, a volume of interest should be defined. The gray and white matter within the lenticulostriate arterial distribution could serve as a confined target for MRS to aid in assessment of extent of injury, prediction of outcomes, and longitudinal evaluations. Further, because the lenticulostriate distribution is readily accessible via the MCA and ACA by vascular catheterization, this disorder should be considered a candidate for acute intervention, i.e., local, endovascular administration of neuroprotective agents.

4.4. Limitations

A major challenge for structural damage detection using VBM is to balance the spatial normalization of structures needed for group comparisons with preservation of the underlying signal. In other words, transformation of individual-subject image data is necessary for disease versus control group contrasts, but the process itself may alter or abrogate the signal from the native tissue (Ashburner and Friston, 2000). Additionally, a prominent criticism of VBM interpretation is that the pattern of statistically significant results could reflect not only atrophy in the tissue of interest, but also indirectly, baseline anatomical differences. Although this principally involves misalignment of gyri/sulci or distinct cortical folding patterns, ventricular misalignment occurs and may be more pertinent for our study (Good et al., 2001).

The sample sizes used in our analyses are admittedly small: 10 ABI children and 9 neurotypical controls. Larger samples would offer greater confidence in our findings as reflective of the population of interest. Despite this, the highly convergent gray and white matter VBM results clearly demonstrate consistent between-group morphological differences to quite high levels of statistical significance. Such robust results in spite of a small sample size and nearly normal MRI in 50% of subjects likely reflect strong disease-specific processes and the considerable homogeneity of the type and age of anoxic insult in our patient group.

Finally, we interpret our findings as specific to pediatric ABI from nonfatal drowning. The observed susceptibility for the lenticulostriate distribution may well be age-specific and not generalize to other ABI etiologies and age groups.

5. Conclusion

This study provides the first quantitative, data-driven, whole-brain (voxel-wise) account of regional gray and white matter loss in pediatric patients with post-drowning ABI. Using VBM methods, structural damage in ABI patients was found to be highly convergent in the central subcortical region, implicating critical motor-system gray and white matter components. Relative sparing of the rest of the neural tissue was observed. This distribution of gray and white matter damage reflects the vascular territory of deep perforating vessels (predominantly the lenticulostriate arteries), proposing their implication in the pathophysiology of anoxic injury with drowning. Together, these findings raise the hypothesis that children with drowning-related ABI suffer from primary motor-system damage and may retain greater global abilities than they can physically express. Future diagnostic and therapeutic considerations are prompted by our findings.

Disclosure of conflicts of interest

The authors have no conflicts of interest to report. We confirm that we have read the Journal's position on issues involved in ethical publication and affirm that this report is consistent with those guidelines.

Acknowledgments

The authors thank Aneil S. Razvi, BFA, for his assistance in preparation of the figures, and all families for their participation in this research study. Funding was provided by the Kronkosky Charitable Foundation (P.T.F., PI) and the NIH — R01 MH074457 (P.T.F., PI); TL1 awards from the NIH/NCATS — UL1 TR001119 supported Mariam Ishaque and Janessa H. Manning. The Conrad Smiles Fund (www.conradsmiles.org) publicized this study and provided funding for travel and logistical support. Miracle Flights for Kids supported airfare costs where possible.

References

Anderson, J.C., Costantino, M.M., Stratford, T., 2004. Basal ganglia: anatomy, pathology, and imaging characteristics. Curr. Probl. Diagn. Radiol. 33 (1), 28–41.

Andersson, J.L.R., Jenkinson, M., Smith, S.M., 2007. Non-linear Registration, aka Spatial Normalization. FMRIB technical report TR07JA2.

Aragao, Mde F., Law, M., Netto, J.P., Valenca, M.M., Naidich, T., 2009. Prognostic value of proton magnetic resonance spectroscopy findings in near drowning patients: reversibility of the early metabolite abnormalities relates with a good outcome. Arq. Neuropsiquiatr. 67 (1), 55–57.

Ashburner, J., Friston, K.J., 2000. Voxel-based morphometry—the methods. NeuroImage 11 (6 Pt 1), 805–821.

Borse, N.N., Gilchrist, J., et al., 2008. CDC Childhood Injury Report: Patterns of Unintentional Injuries among 0–19 Year Olds in the United States, 2000–2006. Atlanta (GA), Centers for Disease Control and Prevention, National Center for Injury Prevention and Control.

Busl, K.M., Greer, D.M., 2010. Hypoxic-ischemic brain injury: pathophysiology, neuropathology and mechanisms. NeuroRehabilitation 26 (1), 5–13.

Christensen, D.W., Jansen, P., Perkin, R.M., 1997. Outcome and acute care hospital costs after warm water near drowning in children. Pediatrics 99, 715–721.

Coupé, P., Manjon, J.V., Gedamu, E., Arnold, D., Robles Collins, M.D., 2010. Robust rician noise estimation for MR Images. Med. Image Anal. 14 (4), 483–493.

Coupé, P., Yger, P., Prima, S., Hellier, P., Kervrann, C., Barillot, C., 2008. An optimized blockwise nonlocal means denoising filter for 3-D Magnetic resonance images. IEEE Trans. Med. Imaging 27 (4), 425–441.

Djulejic, V., Marinkovic, S., Georgievski, B., et al., 2015. Clinical significance of blood supply to the internal capsule and basal ganglia. J. Clin. Neurosci. (Epub ahead of print).

Djulejic, V., Marinkovic, S., Malikovic, S., et al., 2012. Morphometric analysis, region of supply and microanatomy of the lenticulostriate arteries and their clinical significance. J. Clin. Neurosci. 19 (10), 1416–1421.

Douaud, G., Smith, S., Jenkinson, M., et al., 2007. Anatomically related grey and white matter abnormalities in adolescent-onset schizophrenia. Brain 130 (Pt 9), 2375–2386.

Good, C.D., Johnsrude, I.S., Ashburner, J., et al., 2001. A voxel-based morphometric study of ageing in 465 normal adult human brains. NeuroImage 14 (Pt 1), 21–36.

Gutierrez, L.G., Rovira, A., Portela, L.A., et al., 2010. CT and MR in non-neonatal hypoxic-ischemic encephalopathy: radiological findings with pathophysiological correlations. Neuroradiology 52 (11), 949–976.

Hegde, A.N., Mohan, S., Lath, N., Tchoyoson Lim, C.C., 2011. Differential diagnosis for bilateral abnormalities of the basal ganglia and thalamus. Radiographics 31 (1), 5–30.

Huang, B.Y., Castillo, M., 2008. Hypoxic-ischemic brain injury: imaging findings from birth to adulthood. Radiographics 28 (2), 417–439.

Ibsen, L.M., Koch, T., 2002. Submersion and asphyxial injury. Crit. Care Med. 30 (11), S402–S408.

Kriel, R.L., Krach, L.E., Luxenberg, M.G., Jones-Saete, C., Sanchez, J., 1994. Outcome of severe anoxic/ischemic brain injury in children. Pediatr. Neurol. 10, 207–212.

Lancaster, J.L., Rainey, L.H., Summerlin, J.L., Freitas, C.S., Fox, P.T., Evans, A.C., et al., 1997. Automated labeling of the human brain: a preliminary report on the development and evaluation of a forward-transform method. Hum. Brain Mapp. 5, 238–242.

Lancaster, J.L., Woldorff, M.G., Parsons, L.M., Liotti, M., Freitas, C.S., Rainey, L., et al., 2000. Automated Talairach Atlas labels for functional brain mapping. Hum. Brain Mapp. 10, 120–131.

Lu-Emerson, C., Khot, S., 2010. Neurological sequelae of hypoxic-ischemic brain injury. NeuroRehabilitation 26 (1), 35–45.

Momjian-Mayor, I., Baron, J.C., 2005. The pathophysiology of watershed infarction in internal carotid artery disease: review of cerebral perfusion studies. Stroke 567–577.

Mori, S., Wakana, S., Nagae-Poetscher, L.M., van Zijl, P.C.M., 2005. MRI Atlas of Human White Matter. Elsevier, Amsterdam, The Netherlands.

Nucci-Da-Silva, M.P., Amaro, E., 2009. A systematic review of magnetic resonance imaging and spectroscopy in brain injury after drowning. Brain Inj. 23 (9), 707–714.

Rabinstein, A.A., Resnick, S.J., 2009. Practical Neuroimaging in Stroke: a Case-Based Approach. Elsevier Health Sciences, Philadelphia (Print).

Rafaat, K.T., Spear, R.M., Kuelbs, C., Parsapour, K., Peterson, B., 2008. Cranial computed tomographic findings in a large group of children with drowning: diagnostic, prognostic, and forensic implications. Pediatr. Crit. Care Med. 9 (6), 567–572.

Saenz, R.C., 2005. The disappearing basal ganglia sign. Radiology 234, 242–243.

Segonne, F., Dale, A.M., Busa, E., Glessner, M., Salat, D., Hahn, H.K., Fischl, B., 2004. A hybrid approach to the skull stripping problem in MRI. NeuroImage 22, 1060–1075.

Smith, S.M., Nichols, T.E., 2009. Threshold-free cluster enhancement: addressing problems of smoothing, threshold dependence and localisation in cluster inference. NeuroImage 44 (1), 83–98.

Smith, S.M., Jenkinson, M., Woolrich, M.W., Beckmann, C.F., et al., 2004. Advances in functional and structural MR image analysis and implementation in FSL. NeuroImage 23 (Suppl. 1), S208–S219.

Souminen, P.K., Vähätalo, R., 2012. Neurologic long term outcome after drowning in children. SJTREM 20, 55–62.

Topjian, A.A., Berg, R.A., Bierens, J.J.L.M., Branche, C.M., et al., 2012. Brain resuscitation in the drowning patient. Neurocrit. Care. 17 (3), 441–467.

Wardlaw, J.M., 2005. What causes lacunar stroke? J. Neurol. Neurosurg. Psychiatry 76, 617–619.

Weiss, J., 2010. Prevention of drowning. Pediatrics 126 (1), e253–e262.